10R.4 DETAILED COMPARISON OF OBSERVED AND MODELED TORNADOGENESIS

Donald W. Burgess and David C. Dowell
Cooperative Institute for Mesoscale Meteorological Studies, University of Oklahoma/NSSL, Norman, OK

Louis J. Wicker and Arthur Witt
NOAA/National Severe Storms Laboratory

1. INTRODUCTION

This paper describes a research project that is part of a larger effort to study/model many aspects of the Oklahoma City supercell and tornado of 8 May 2003. Previous work has been: 1) examination of the structure and evolution of the supercell storm (Burgess 2004), utilizing data from the central-Oklahoma WSR-88D (KTLX), 2) assimilation of radar (and other) observations and numerical modeling of the storm (Dowell *et al*. 2004a, hereafter D04), utilizing research WSR-88D data (KOUN), and 3) high resolution storm-scale model experiments of tornadogenesis (Wicker and Dowell 2004)

The research effort reported here examines the time interval of the formation of the violent (F4) tornado from the 8 May supercell and compares high-resolution model output to high-resolution radar observations. The high-resolution storm-scale analyses are generated through assimilating KOUN single-Doppler and reflectivity observations into a cloud model using the ensemble Kalman filter methodology described in Snyder and Zhang (2003) and Dowell *et al*. (2004a,b).

2. DATA SOURCES

a. KOUN ASSIMILATION METHODOLOGY

Volume scans of Doppler velocity and effective reflectivity factor (hereafter "reflectivity") of the Oklahoma City storm were obtained by the KOUN radar approximately every 6 min. Dual-polarization measurements were also collected but are not used in this study. Each elevation scan between 2046 and 2209 (all times are UTC) is assimilated into the model (There are 187 scans, representing 14 volumes). These observations document the early stages of the Oklahoma City storm's life cycle (see Fig. 1 from D04) to the time of tornadogenesis at ~2208. Before objectively analyzing the observations, we removed contaminated data (ground clutter, range folding, etc.) and unfolded aliased Doppler velocities. Maintaining the conical shape of each sweep (to eliminate vertical interpolation), a Cressman scheme with a 1000-m radius of influence is used to analyze Doppler velocity and reflectivity at grid points 2000-m apart in the plane of the sweep (D04).

The numerical cloud model used for the data-assimilation and forecast experiments is the NSSL Collaborative Model for Multiscale Atmospheric Simulation (NCOMMAS). A brief description of the model can be found in DO4. The experiment here uses the modified (Gilmore *et al.* 2004) Lin-Farley-Orville (LFO) scheme, which includes four hydrometeor classes: rain, ice crystals, snow, and hail/graupel.

The analysis employs a moving grid consisting of 201 grid points (100 km) in each horizontal direction and 61 grid points (18 km) in the vertical direction. The horizontal grid spacing is uniformly 0.5 km, whereas the vertical grid spacing varies from 0.1 km in the lowest 1 km AGL to 0.7 km near the grid top. The grid origin is at the KOUN radar site, and the grid is positioned so that initial storm development occurs in the central part of the domain.

The initialization of each member of the 50-member forecast ensemble begins with the unmodified 0Z 9 May 2003 Norman, Oklahoma sounding. Then, random sinusoidal perturbations are added to each member's vertical profile of temperature, dewpoint, and horizontal wind components (W. Skamarock and C. Snyder 2004, personal communication). The motivation for adding these perturbations is uncertainty in the environmental conditions. Warm bubbles at random locations within a limited portion of the domain are then added to each ensemble member; the region where the perturbations are added includes the region where radar echoes actually developed near the dryline. Unlike D04, the ensemble is initiated at the time of first echoes. The convective initiation mechanism in our experiment is artificial because the dryline is not actually modeled.

Both Doppler velocity (Dowell *et al.* 2004b) and reflectivity observations (D04, Tong and Xue 2005) are assimilated into the model. Observation errors are assumed to be 2 m s^{-1} and 5 dBZ for Doppler velocity and reflectivity, respectively. Although the latter error magnitude seems unrealistically large, we find that it is helpful to assume a large error magnitude when assimilating

reflectivity observations. Observations are processed serially (that is, one at a time), and all model fields except pressure and the mixing coefficient are updated each time an observation is processed. Reflectivity corresponding to the model fields is computed with the equations suggested by Smith *et al*. (1975), in a manner similar to Tong and Xue (2005). No ensemble inflation is employed during the assimilation. Other details of the EnKF assimilation scheme are provided by D04.

For the analysis shown here, we choose to use the mean fields generated by the ensemble, e.g., all 50 members are averaged together to create the analysis at a given time. The resulting analysis will therefore be rather smooth as most of the small-scale information present in each individual member is averaged out. However, given our current state of knowledge, use of the mean fields is a reasonable starting point. Further research is currently underway at NSSL examining how to better use the ensemble information in storm-scale analyses.

b. TDWR RADAR CHARACTERISTICS

FAA operates the OKC TDWR, a C-band Doppler weather radar. It is sensitive, high-resolution radar with 0.5^{o} beamwidth and 150 m gate spacing (see Istok *et al*. 2005 for information on the radar and its upcoming use by NWS forecasters). During severe weather situations (Hazardous Weather Mode), the scan strategy features one or more 0.5^{o} elevation angles each minute and a total volume scan time of three minutes with a maximum elevation angle of 28^{o}. The southeast Oklahoma City metro location of the radar gave it an ideal vantage point from which to observe tornadogenesis, which occurred at 5 to 10 km range northwest of the radar.

c. WDSSII MULTI-DOPPLER SOFTWARE

The Warning Decision Support System – Integrated Information (WDSSII) has been developed by NSSL to support research development and display (Hondl 2003). As part of NSSL's research emphasis on multi-sensor/multi-radar techniques, a new multi-Doppler module has been developed to derive and display 3D wind fields (Witt *et al*. 2005). For the research presented here, the new capability has been utilized to calculate dual-Doppler winds from KTLX WSR-88D and OKC TDWR radar data. The necessary minimum angle between radar beams (20^{o}) and storm location, limits the time period of analysis to 2206 and beyond.

WDSSII was also used to display and analyze the TDWR data and the model-simulated TDWR data (explained above in (a) and (b)).

3. COMPARISON OF TDWR AND MODEL DATA

Two types of comparisons have been done. First is a comparison of horizontal wind fields between a more traditional dual-Doppler analysis and the model output from the data assimilation. As expected given the nature of the assimilation scheme described above, model output compares well to radar observations. A comparison of low-level vector wind fields (Fig. 1) illustrates the generally good agreement between the model (assimilating KOUN data) and dual-Doppler winds constructed from TDWR and KTLX data. A few differences are worth noting. First, even with an attempt to maximize the number of dual-Doppler vectors (produced by choosing a relatively small angle between radar beams) and having sensitive radars at close range to the storm, the model analysis has a definite advantage in providing a more complete wind field. Such advantage will be important in later stages of the project as trajectories and other diagnostics are computed. Second, small areas of missing reflectivity/wind output are noted (black areas in Fig. 1a) whereas the model outputs are continuous. The missing data arise from ground-clutter contamination, blockage by tall objects near TDWR, and residual second-trip echo. Finally, in the area of the developing tornado (inside tip of the hook echo; (-8,10) model coordinates in Fig. 1b) and other areas (not shown), wind-field gradients are stronger in the dual-Doppler field than in the model field. This difference results from the scale of the model assimilation and other model aspects and will be the subject of additional future experimentation, and possible errors in dual-Doppler vector calulation.

Another comparison of model and dual-Doppler wind fields is offered in Fig. 2, this time for a higher height within the storm. The same general agreement between model and dual-Doppler winds appears. However, there are a few differences from the low-level comparison. First and most obvious is that the dual-Doppler winds no longer have the higher gradients. In fact, the dual-Doppler winds are very smooth, greatly reducing gradients. This arises from the nature of the TDWR scan strategy and closeness of the storm to the radar. Small analysis radii of influence (used in Fig. 1b) produce coverage gaps between observed elevation angles and bands of missing data on constant-level surfaces. To produce useful output, the analysis radii of influence must be significantly enlarged, producing overly smoothed vector fields. The model output does not suffer from similar loss of resolution. One of the areas where the loss of resolution is important is within the bounded weak echo region where the dual-Doppler flow

curvature is much reduced when compared to the model.

The second type of comparison between the model and TDWR is to analyze model data that have been transformed into simulated TDWR data. The model fields, with assimilated KOUN radar observations, were sampled by a simulated radar at the TDWR location, employing a sampling strategy like that of TDWR. For simplicity, point estimates of the model fields computed by trilinear interpolation, rather than power-weighted means, were used to produce these simulated TDWR data. As shown in Fig. 3, the simulated TDWR data compare well with actual TDWR data. Both the mesocyclone and tornado cyclone signatures are observed in the simulated data in approximately the same locations as seen in the TDWR observations. For the particular elevation shown, the model only partially resolves the tornado cyclone. Qualitatively evident in the same figure is the somewhat reduced magnitude of the simulated velocities. This is more apparent in the quantitative comparison shown in Fig. 4. In general, the same trends in mesocyclone and tornado cyclone rotation velocities are seen (including the time of the appearance of the tornado cyclone), but the magnitudes are reduced. These differences are a topic of future research. Among the possible causes of the model-reduced magnitudes are the scale of the KOUN assimilation input and the use of ensemble mean output. Individual or groups of ensemble members might better represent the TDWR observations.

A comparison of model and TDWR reflectivity has also been performed (Fig. 5). Model mid-level maximum reflectivity (as illustrated by the 5-km values) agrees fairly well with TDWR 5-km values although the model reflectivity is slightly (higher) lower than the observations at (earlier) later times. Low-level model maximum reflectivity (as illustrated by the 1-km values) is considerably less than the observations, sometimes by as much as 10 dBZ. Current model microphysical parameterization and reflectivity calculation equations are likely causes of some of the differences, as is the possibility of a low bias in KOUN data when compared to the other radars. Additional research will be performed in this area, including more advanced microphysical modules, assimilation of dual-polarization parameters, and further investigation of KOUN reflectivity.

4. DISCUSSION

The overall evolution of the storm and the tornado was discussed by Burgess (2004) and will only be summarized here. After a somewhat complicated multi-cell organizing stage (including left-moving splitting cells), the supercell became well organized about 2140 (all times are UTC), strengthened until tornado time (2200-2238), and weakened thereafter. During the pre-tornadic phase, the storm maintained strong and strengthening mesocyclone-scale rotation aloft and strengthening convergence at cloud base. Near the time of tornadogenesis, low-level rotation rapidly increased.

The availability of higher-resolution (in time and space) TDWR and model data provides opportunity to better examine the pre-tornadic time period. The TDWR radar data are of such high resolution (<1^o effective beamwidth and <10 km range, 150 m gate spacing, and 1 or more 0.5^o scans every minute) that they are comparable to recent data collection by some portable Doppler radars (Wurman and Gill 2000). The time/height evolution of the mesocyclone, tornado cyclone, and tornado signature as seen by TDWR (Fig. 6a) indicates rapid changes occurring about 2200. The mesocyclone rotational velocity aloft slowly strengthens and the mesocyclone base slowly lowers toward the surface between 2140 and 2200 (also see Burgess *et al* 2004 for a more complete graph of rotational velocity for all storm heights and times). Just before 2200, the mesocyclone begins strengthening more rapidly and it quickly becomes defined at low levels. The low-level mesocyclone signature just after 2200 is a combination of strong convergence (which has been increasing since 2140; not shown in this paper, see Burgess 2004) and rotation. At the same time, a signature smaller than the mesocyclone, the tornado cyclone, is detected almost simultaneously through a deep column, but with maximum rotational velocity near 2.5 km AGL. During this time interval, mesocyclone diameter remains at ~5 km and tornado cyclone diameter is ~2 km. The two co-existing vortex signature diameters are annotated in Fig 3a.

The tornado signature [defined as shear associated with the tornado and a diameter of <1 km, but not necessarily sampled as the gate-to-gate shear of a Tornadic Vortex Signature (TVS)] appears first at low levels at ~2205. The tornado signature quickly develops upward through a deep column and strengthens. At heights/times where it appears, it replaces the tornado cyclone signature. The two signatures are not both well defined on any of the same scans. This suggests the possibility that the tornado cyclone is an intermediate stage leading to tornado development. Davies-Jones and Wood (2005), experimenting with a time-dependent Burgers-Rott vortex, have simulated a similar evolution. A tornado cyclone, once formed and continuing within low-level convergence and updraft,

can converge into a tornado in a few minutes…similar to the May 8 TDWR observations.

The evolution seen in the TDWR observations is also detected in the model (Fig. 6b). With the caveat of the differences mentioned in the previous section (weaker magnitudes), the model generally displays the same evolution. An exception is close to the ground (lowest 500 m) where all winds, including mesocyclone and tornado cyclone rotational velocities, are considerably weaker. The model generates no tornado-scale signature. A finer numerical grid than used here would be required to generate a tornado-like vortex in the model.

As is usual with tornado-related research, comparison of radar data with reported ground damage is somewhat ambiguous. A short-lived, weak, transient tornado is reported at 2200, but is not detected in TDWR or model observations. A second tornado (first enclosed contour in Fig. 3) is reported to have occurred between 2004 and 2008, and a third tornado (the F4 tornado; second enclosed contour in Fig. 3) is listed as beginning at 2210 and continuing 28 minutes. TDWR data strongly suggest that, based on location, the tornado forms slowly between 2204 and 2210, but is a continuous tornado-scale circulation from its beginning, with no gap being detected.

5. CONCLUSIONS AND FUTURE WORK

For the May 8 case, a radar (TDWR) very close to the storm detects many tornadogenesis details with high time and space resolution. A tornado cyclone develops within the mesocyclone and transitions into a tornado signature. A numerical model is used to assimilate radar observations from another nearby radar (but one with less resolution) and forecast storm reflectivity and velocity. Model fields somewhat replicate TDWR observations, but velocity magnitudes are less, particularly at low levels, and no tornado signature is produced.

The May 8th project will continue and future work is planned in several areas. There will be additional numerical model experiments with different microphysics, different assimilation procedures, and other changes. TDWR observations and model output will be used to further diagnose the tornadogenesis process. The origin of the tornado cyclone, including vorticity sources and trajectories, will be further studied. Additional ultra-high resolution storm-scale forecasts of tornadogenesis are planned.

Work to date suggests that there might be some operational value in detecting precursors to tornadogenesis with model fields available in real time from assimilation/model schemes like the one being used here. For example, time/height profiles of convergence, vertical velocity, and vorticity might be quite valuable for either human or algorithm evaluation leading to anticipation of tornadogenesis.

6. ACKNOWLEDGMENTS

This conference paper was prepared with partial funding provided by the NOAA/Office of Oceanic and Atmospheric Research under NOAA-University of Oklahoma Cooperative Agreement #NA17RJ1227, U.S. Department of Commerce. The statements, findings, conclusions, and recommendations are those of the authors and do not necessarily reflect the views of NOAA of the U.S. department of Commerce. The second author was supported by National Science Foundation Grant ATM-0333872. We thank Kevin Scharfenberg and Gordon Carrie for help in working with the KOUN data.

7. REFERENCES

Burgess, D.W, 2004: High resolution analyses of the 8 May 2003 Oklahoma City storm, Part I: Storm structure and evolution from radar data. CD-ROM, *22nd Conf. Severe Local Storms*, Hyannis, MA, AMS, Paper # 12.4.

Davies-Jones, R.P., and V.T.Wood, 2005: Simulated Doppler velocity signatures and evolving tornado-like vortices. This conference.

Dowell, D. C., L. J. Wicker, and D. J. Stensrud, 2004a: High resolution analysis of the 8 May 2003 Oklahoma City storm. Part II: EnKF data assimilation and forecast experiments. CD-ROM, *22nd Conf. Severe Local Storms*, Hyannis, MA, AMS, Paper # 12.5.

Dowell, D. C., F. Zhang, L. J. Wicker, C. Synder, and N. A. Crook, 2004b: Wind and temperature retrievals in the 17 May 1981 Arcadia, Oklahoma supercell: Ensemble Kalman filter experiments. *Mon. Wea. Rev.*, **132,** 1982-2005.

Gilmore, M. S., J. M. Straka, and E. N. Rasmussen, 2004: Precipitation and evolution sensitivity in simulated deep convective storms: Comparisons between liquid-only and simple ice and liquid phase microphysics. *Mon. Wea. Rev.*, **132**, 1897-1916.

Hondl, K.D., 2003: Capabilities and components of the Warning Decision Support System-Integrated Information (WDSSII). CD-ROM, *19th Intnl. Conf. on Interactive Information and Processing Systems (IIPS)*, Long Beach, CA, AMS, Paper #14.7.

Istok, M.J., P. Pickard, R. Okulski, R.E. Saffle, and B. Bumgarner, 2005: NWS use of FAA radar data – progress and plans. This conference.

Smith, P.L., Jr., C.J. Myers, and H.D. Orville, 1975: Radar reflectivity factor calculations in numerical cloud models using bulk parameterization of precipitation. *J. Appl. Meteor*., **14**, 1156-1165.

Snyder, C., and F. Zhang, 2003: Assimilation of simulated Doppler radar observations with an ensemble Kalman filter. *Mon. Wea. Rev.*, **131**, 1663-1677.

Tong, M., and M. Xue, 2005: Ensemble Kalman filter assimilation of Doppler radar data with a compressible nonhydrostatic model: OSS Experiments. *Mon. Wea. Rev*., **133,** 1789–1807.

Wicker, L.J., and D.C. Dowell, 2004: High-resolution analysis of the 8 May 2003 Oklahoma City storm. Part III: An ultra-high resolution forecast experiment. CD-ROM, *22nd Conf. Severe Local Storms*, Hyannis, MA, AMS. Paper #12.6

Witt, a., R.A. Brown, and V. Lakshmanan, 2005: Real-time calculation of horizontal winds using multiple Doppler radars: A new WDSSII module. This conference.

Wurman, J., and S. Gill, 2000: Finescale observations of the Dimmit, Texas (2 June 1995), tornado. *Mon. Wea. Rev*. **128**, 2135-2164.

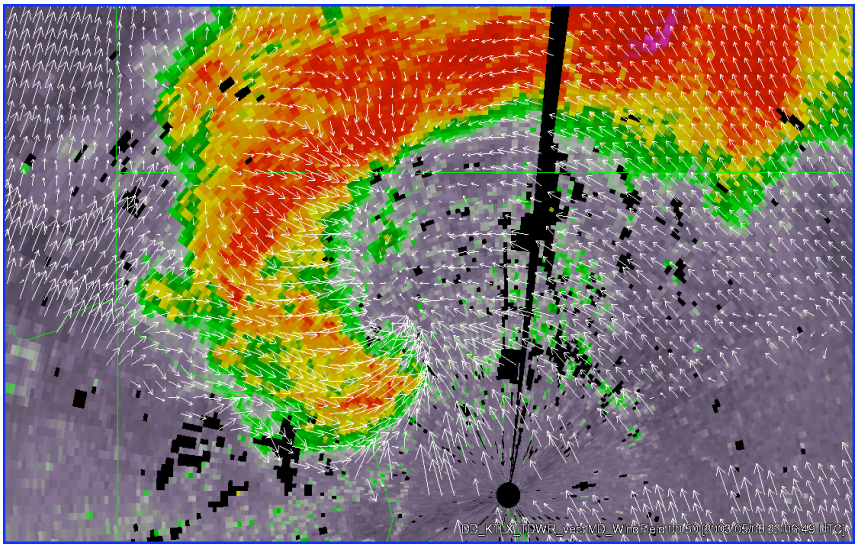

a.

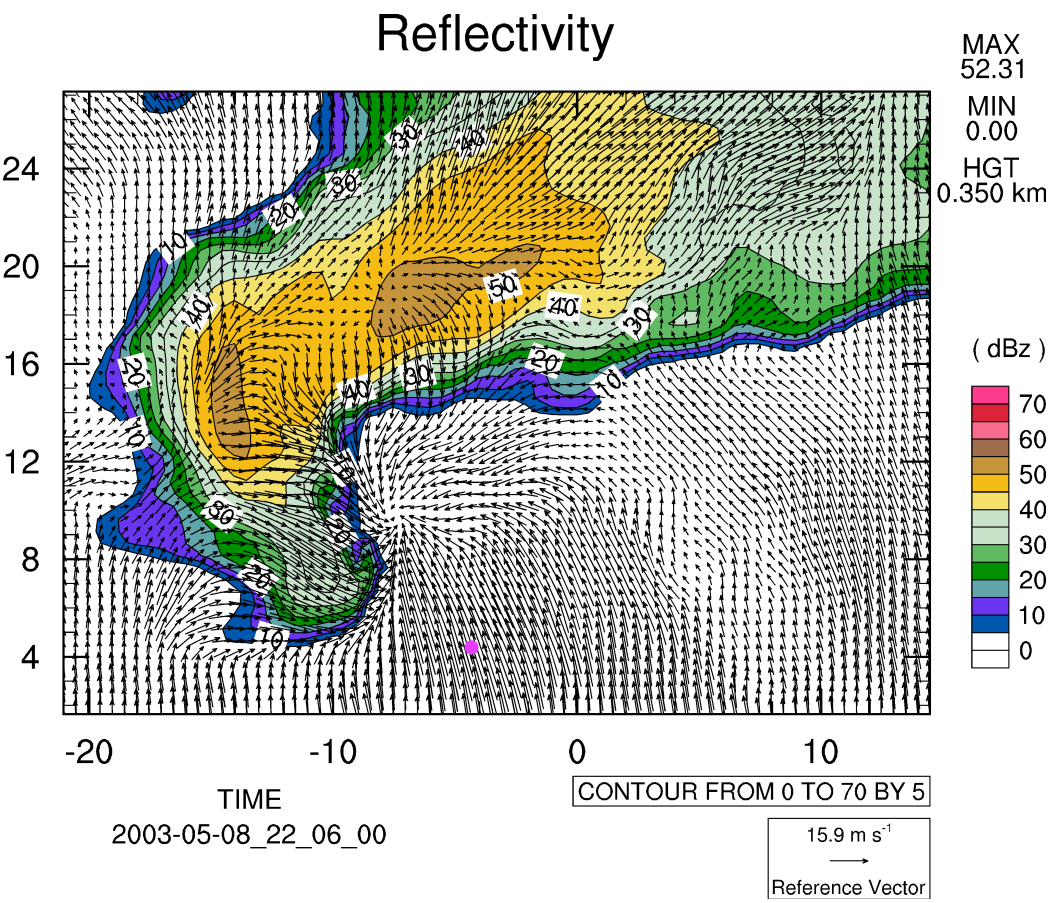

b.

Figure 1. Low-level ground-relative wind vectors overlaid on reflectivity at 2206 UTC for a) KTLX and TDWR dual-Doppler winds and TDWR 0.5° reflectivity, and b) numerical model winds and derived reflectivity. For Reflectivity color scale in (a), see Fig. 3. Dark colored circle in (b) is location of TDWR radar.

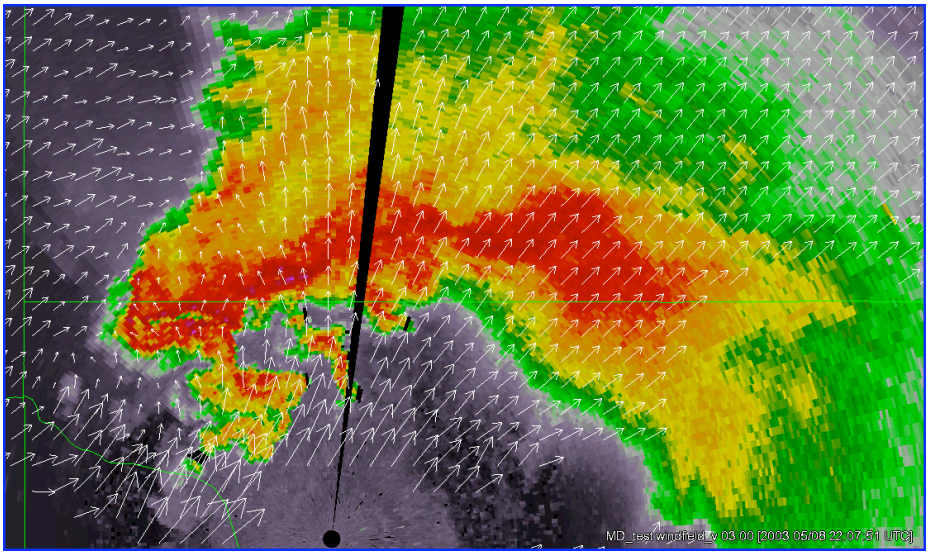

a.

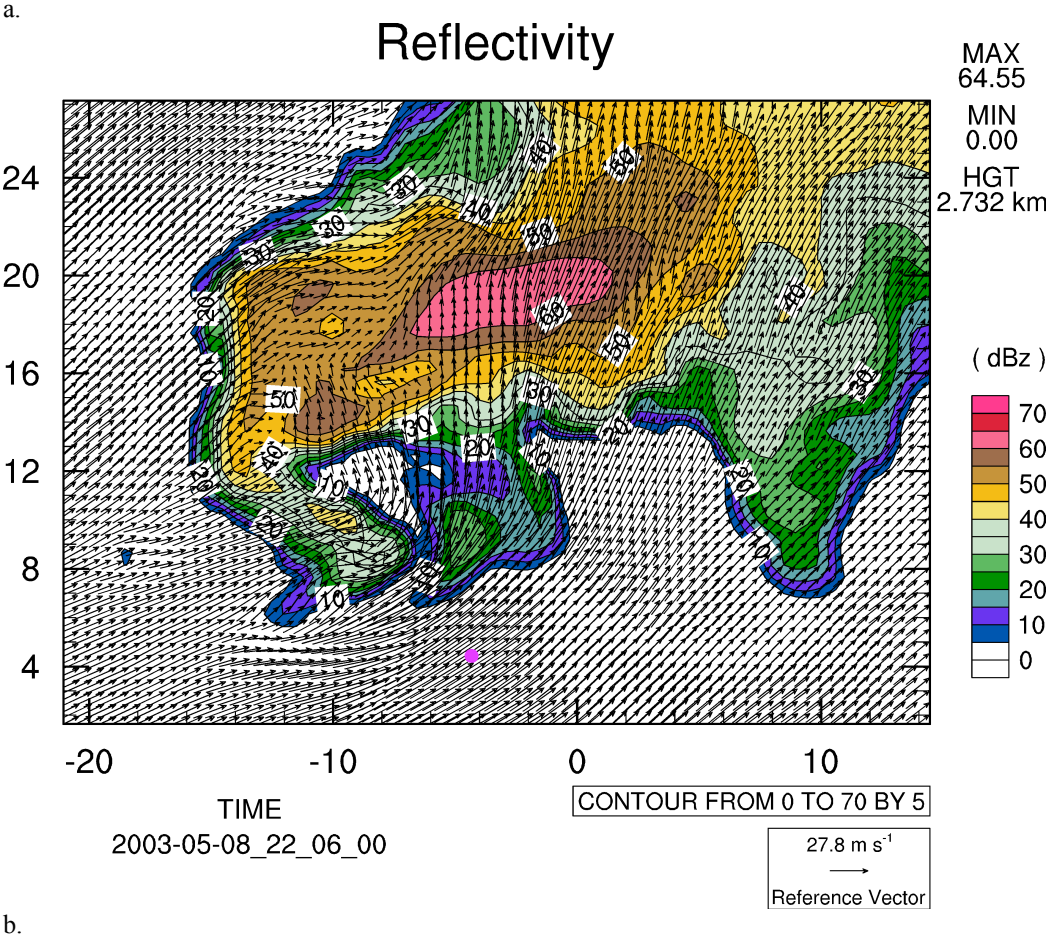

b.

Figure 2. Same as Fig. 1 except for 2.7 km AGL.

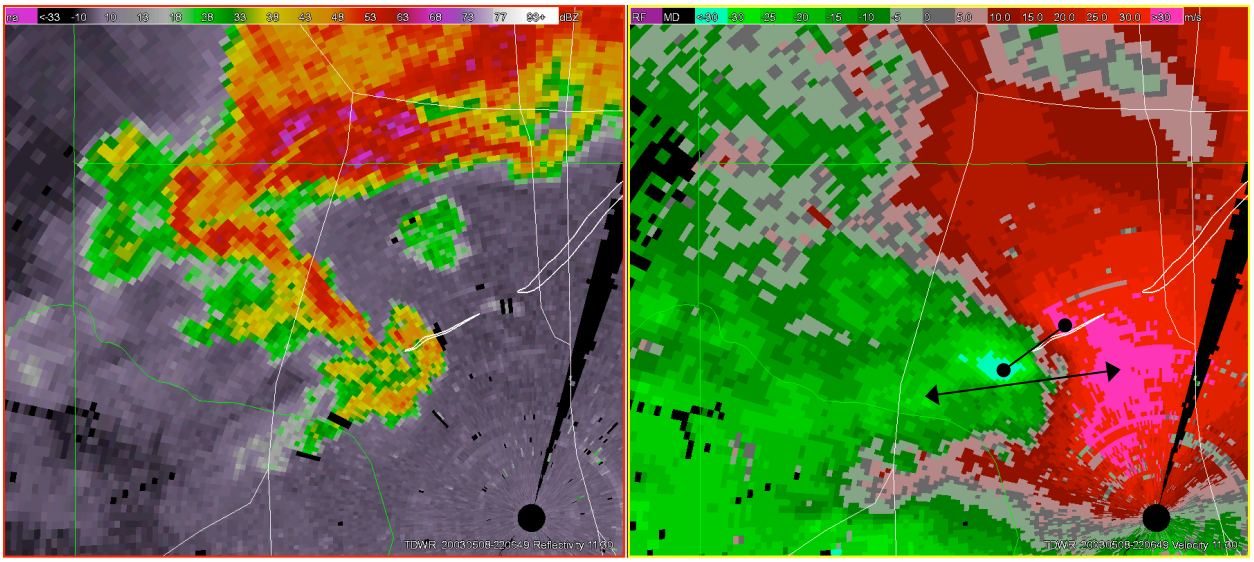

a.

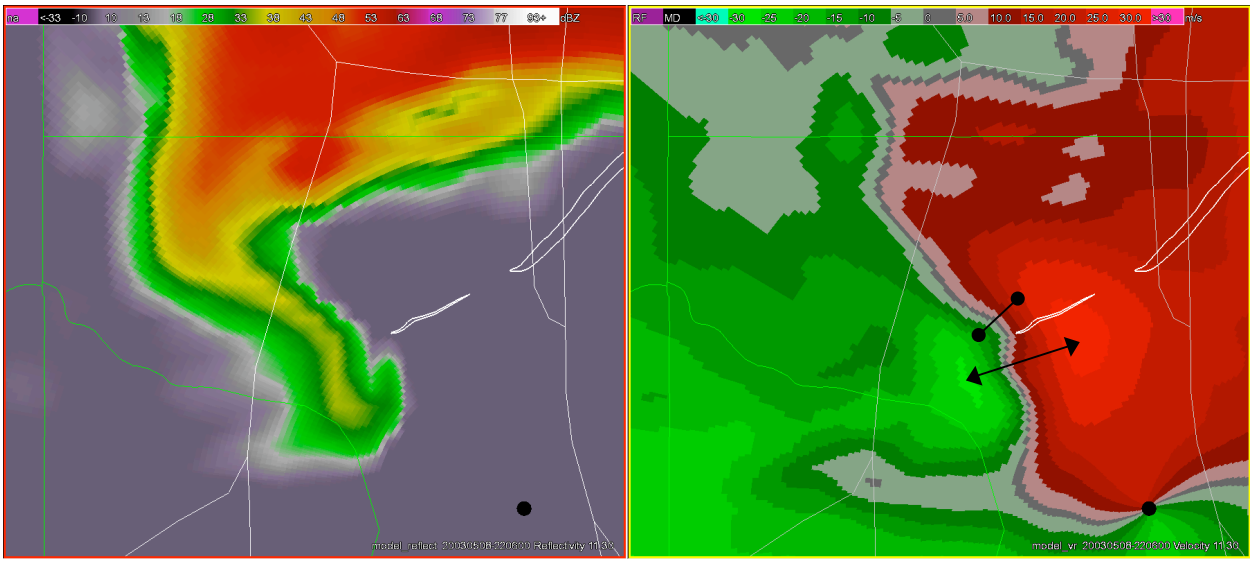

b.

Figure 3. Reflectivity (left) and radial velocity (right) for (a) TDWR and (b) numerical model at 11.3^{o} elevation angle, 2206 UTC. Annotated lines on radial velocity mark diameter of mesocyclone (dark arrows) and tornado cyclone (dark circles). Thick white contours are tornado damage areas and dark circle is TDWR location. At the range of the circulations, the height above ground is about 1.25 km.
location.

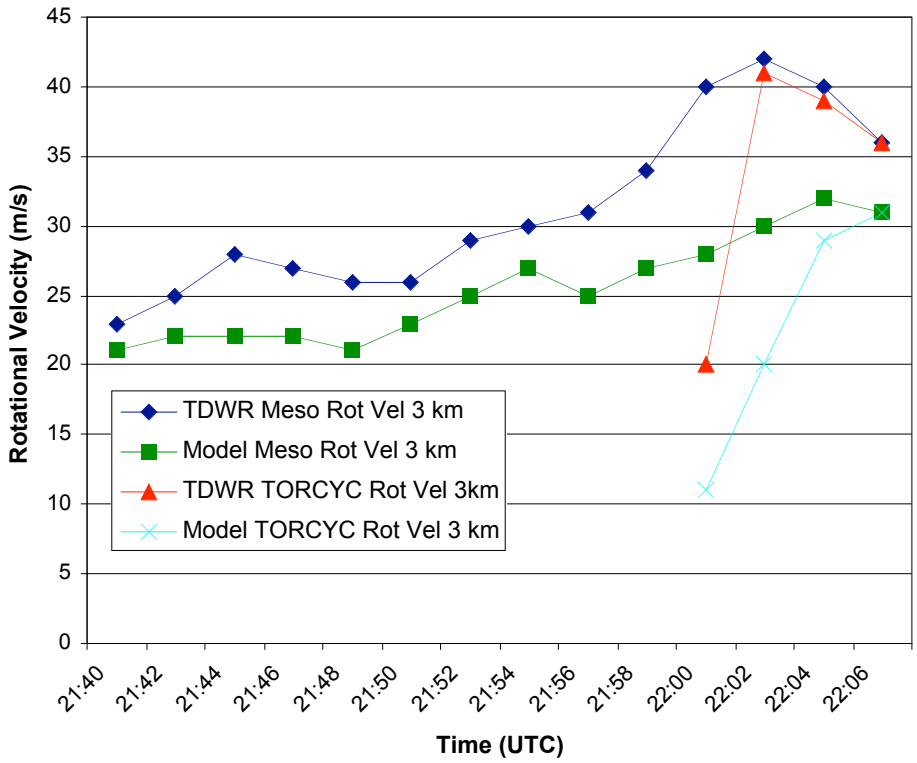

Figure 4. Plot of TDWR and numerical model mesocyclone and tornado cyclone rotational velocity.

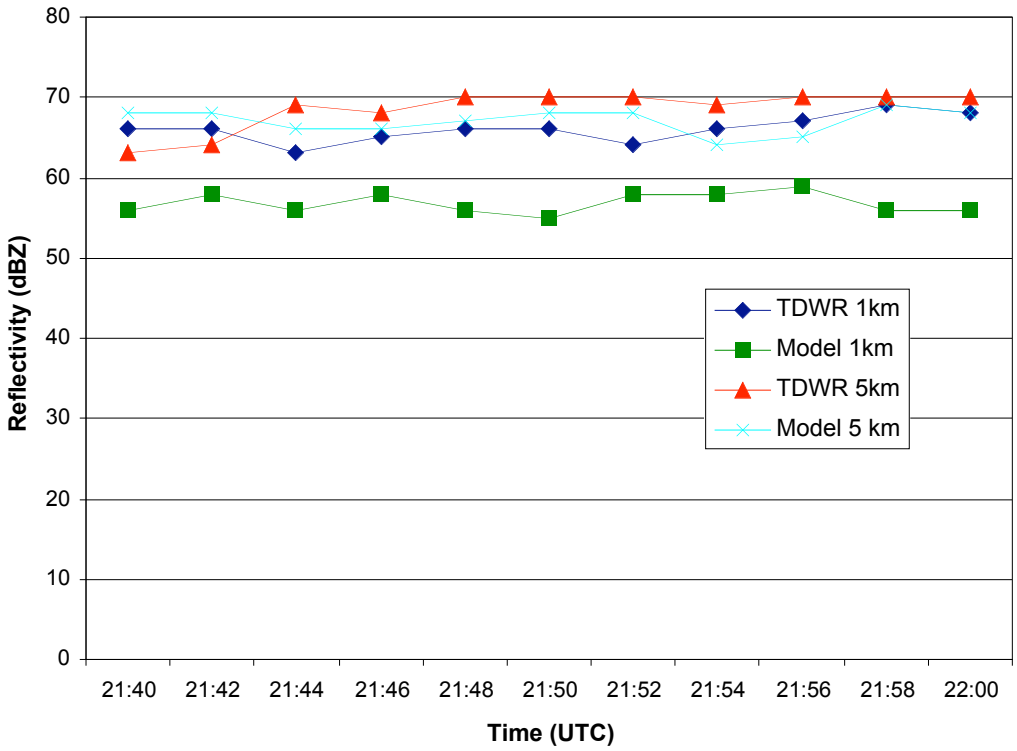

Figure 5. Plot of TDWR and numerical model maximum reflectivity for 1 km and 5 km.

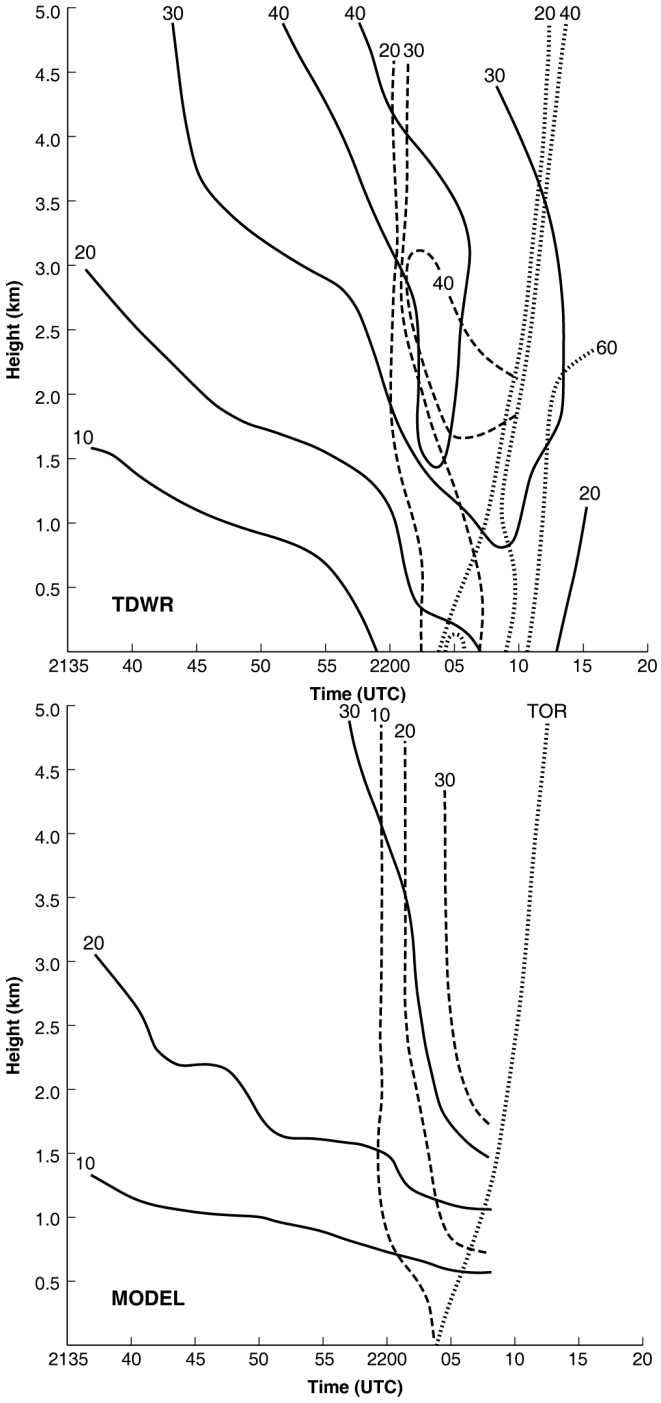

Figure 6. Height/time section for mesocyclone (solid line), tornado cyclone (dashed line), and tornado signature (dotted line) rotational velocity for TDWR (top) and numerical model (bottom). Tornado signature curve for numerical model (labeled TOR) has been added from TDWR data.